Applied Mathematical Modelling 37 (2013) 2051–2062

Contents lists available at SciVerse ScienceDirect

Applied Mathematical Modelling

journal homepage: www.elsevier.com/locate/apm

Modeling of thermal phenomena in single laser beam and laser-arc hybrid welding processes using projection method

W. Piekarska *, M. Kubiak

Institute of Mechanics and Machine Design Foundations, Czestochowa University of Technology, Dabrowskiego 73, 42-200 Czestochowa, Poland

ARTICLE INFO

Article history:
Received 17 February 2012
Received in revised form 18 April 2012
Accepted 27 April 2012
Available online 12 May 2012

Keywords:
Heat transfer
Fluid flow
Welding simulation
Projection method
Laser welding
Hybrid welding

ABSTRACT

This paper concerns mathematical and numerical modeling of thermal phenomena accompanying single laser and laser-arc hybrid butt welding of steel sheets. Coupled heat transfer and fluid flow in the fusion zone were described respectively by transient heat transfer equation and Navier–Stokes equation. Laser beam and electric arc heat sources were modeled using different heat source power distributions. Latent heat associated with the material's state changes, buoyancy forces and liquid material flow through a porous medium were taken into account in considerations. Differential governing equations were numerically solved using projection method combined with finite volume method. Elaborated solution algorithm was implemented into computer solver used for simulation of heat transfer and fluid flow during welding. The geometry of the weld and heat affected zone as well as cooling rates were estimated on the basis of numerically obtained temperature field.

1. Introduction

Laser beam welding has increasing applications in many industries, mainly due to a high welding speed used in the process, good quality of joints and small heat affected zone (HAZ) [1–3]. However, laser welding of steel is accompanied by many phenomena not found in conventional welding methods. The concentration of heat energy leads to the local material evaporation. Moreover, high cooling rates in laser welding contributes to occurring of hardening structures in the weld and HAZ even in susceptible to welding, unalloyed and low-alloy constructional steels. These difficulties as well as the need for a precise fit-up of welded parts (especially when combining elements of large thickness) in some cases limit its application [1]. Therefore, alternative methods are still looked for.

In recent years, particular attention is paid to the laser-arc hybrid welding [4–7]. Laser-arc hybrid welding combines laser beam welding with popular and well-known electric arc welding. In this process deep material penetration is achieved with a good gap filling through the cooperation of electric arc and laser beam in a single process [4]. The combination of laser beam and electric arc allows creating good quality joints that have many advantages in comparison to welds made in a single laser beam welding, even at higher welding speeds [6].

The knowledge about thermal phenomena accompanying welding processes is helpful in estimation of many technological parameters that should be correctly set to ensure process stability and the best possible quality of the joint [7–9]. Thermal phenomena accompanying welding processes are difficult or even impossible to analyze through experimental research. Furthermore, experimental determination of appropriate set of welding processes parameters is expensive and time consuming. Therefore the research is also focused on mathematical modeling and numerical analysis [10–20], which allows for a prediction of chosen process parameters that can be used in practice.

* Corresponding author. Tel.: +48 34 325 06 99; fax: +48 34 325 06 47.
E-mail address: piekarska@imipkm.pcz.pl (W. Piekarska).

0307-904X/$ - see front matter © 2012 Elsevier Inc. All rights reserved.
http://dx.doi.org/10.1016/j.apm.2012.04.052

Modeling of thermal phenomena in welding process using laser beam heat source requires a new approach to the theory and numerical solution techniques, because heat distribution proceeds in different conditions in comparison to classic welding techniques. During laser beam welding the material is heated by highly concentrated heat source to very high temperatures, even reaching the boiling point [2,13,18,19]. The movable heat source with a high power density differs from classical welding and heating sources. Very important in terms of formal modeling is a proper selection of heat source shape and its energy distribution. The new mathematical models describing the distribution of the energy flux taking into account the real conditions are being constantly looked for [7,13,21,22].

Liquid material flow in the fusion zone considered in the computational model allows for the analysis of previously neglected phenomena associated with the dynamics of welding pool formation [11,16,18–20]. Material flow in the welding pool affects calculated temperature distribution in welded element, in consequence having significant influence on numerically estimated shape and size of the weld.

This study contains mathematical and numerical modeling of temperature field with a motion of liquid steel in the welding pool taken into account in single laser beam and laser-arc hybrid welding processes. Coupled heat transfer and fluid flow in the fusion zone are described respectively by transient heat transfer equation with convective term and Navier–Stokes equation. Fuzzy solidification front is assumed in calculations where solid–liquid zone is treated as a porous medium. Latent heat associated with solid–liquid and liquid–gas transformations is taken into account in solution algorithms. Differential governing equations are numerically solved using projection method with finite volume method. Analyzed three-dimensional domain is discretized using staggered grid. On the basis of obtained temperature field, size and shape of the weld and HAZ are determined as well as cooling rates in laser beam and laser-arc hybrid butt welded joints.

2. Mathematical formulation

Heat transfer in welded joint depends on the amount and distribution of heat energy supplied to the workpiece, welding speed and the motion of a liquid material in the welding pool. In a single laser beam welding highly concentrated heat source melts the workpiece causing significant evaporation of the material in heat source activity zone and creating the "keyhole". In laser-arc hybrid welding process two different heat sources (electric arc and laser beam) are acting in tandem [5], changing the mechanism of material melting.

Liquid material motion is mostly driven by the buoyancy forces (Boussinesq's model) in the melted zone. The region between solidus and liquidus temperatures (mushy zone) is treated as the porous medium (Darcy's model) [18,20]. Phase transformations due to material state changes [23,24] are taken into consideration in the mushy zone (solid–liquid transformation) and in temperatures exceeding the metal boiling point (liquid–gas transformation). Modeled thermal phenomena accompanying welding processes as three-dimensional problem are presented in a scheme of the considered system (Fig. 1).

2.1. Governing equations

The temperature field is obtained by the solution of transient heat transfer equation with convective term, expressed as follows:

$$\frac{\partial}{\partial x_i}\left(\lambda\frac{\partial T}{\partial x_i}\right) = C_{ef}\left(\frac{\partial T}{\partial t} + v_i\frac{\partial T}{\partial x_i}\right) - \tilde{Q}, \tag{1}$$

where $T = T(x_i, t)$ is temperature at a point x_i, v_i is a velocity vector, $\lambda = \lambda(T)$ is a thermal conductivity, $C_{ef} = C_{ef}(T)$ is an effective heat capacity with latent heat of fusion and evaporation taken into account, $\tilde{Q}$ is a volumetric heat source with laser beam and electric arc heat sources power distributions taken into considerations.

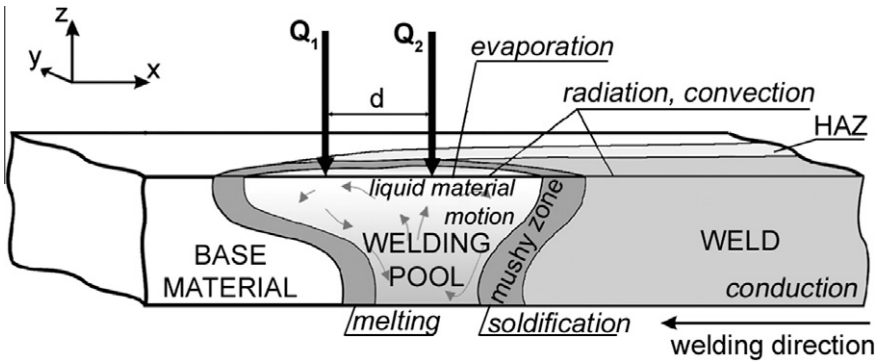

Fig. 1. Scheme of considered phenomena in analyzed system.

Initial condition: $t = 0$, $T = T_0$ and boundary conditions complete Eq. (1), taking into account heat loss due to convection, radiation and evaporation

$$\Gamma : -\lambda\frac{\partial T}{\partial n} = \alpha(T|_\Gamma - T_0) + \varepsilon\sigma(T^4|_\Gamma - T_0^4) - q_o + q_v, \tag{2}$$

where α is convective coefficient, ε is radiation coefficient, and σ is Stefan–Boltzmann constant. Element q_o is the heat flux towards the top surface of the welded element ($z = 0$) in the source activity zone, while q_v represents heat loss due to material evaporation in area where $T \geqslant T_L$, Γ is a boundary of analyzed domain.

Velocity field of liquid material in the melted zone is obtained by the solution of Navier–Stokes equation fulfilling the continuity equation with buoyancy forces and flow through porous medium taken into consideration

$$\frac{\partial \rho}{\partial t} + \frac{\partial}{\partial x_i}(\rho v_i) = 0, \tag{3}$$

$$\frac{\partial(\rho v_i)}{\partial t} + \frac{\partial}{\partial x_j}(\rho v_i v_j) = -\frac{\partial p}{\partial x_i} + \frac{\partial}{\partial x_j}\left(\mu\frac{\partial v_i}{\partial x_j}\right) + \mathbf{g}\beta_T(T - T_{ref}) - \frac{\mu}{\rho K}v_i, \tag{4}$$

where ρ is a density, $\mathbf{g}$ is acceleration of gravity, β_T is a volume expansion coefficient due to heating, T_{ref} is a reference temperature, μ is a dynamic viscosity, K is porous medium permeability.

Eq. (4) is completed by initial condition $t = 0$:$\mathbf{v} = 0$ and boundary conditions implemented at the welding pool boundary determined by solidus temperature ($T_{ref} = T_S$), which are described as follows [17]:

$$\Gamma : \mathbf{v}|_\Gamma = 0, \quad \tau_s = \mu\frac{\partial \mathbf{v}}{\partial n} = \frac{\partial \gamma}{\partial T}\frac{\partial T}{\partial s}, \tag{5}$$

where $\boldsymbol{\tau}_s$ is Marangoni shear stress in the direction tangent to the surface, γ is surface tension coefficient.

Porous medium permeability K in the mushy zone is described by Carman–Kozeny equation [19,20]

$$K = K_0\frac{f_l^3}{(1 - f_l)^2}; \quad K_0 = \frac{d_0^2}{180}, \tag{6}$$

where f_l is a porosity coefficient, d_0 is an average solid particle diameter.

2.2. Laser beam and electric arc heat sources

Heat transfer is mostly affected by the amount and distribution of heat input delivered by the laser beam or laser beam and electric arc in hybrid welding. Defined by Goldak [21] 'double ellipsoidal' power distribution of the heat source bellow the welding arc is often used in modeling of arc welding process. This widely accepted by the researchers heat source model can be used to simulate various arc parameters and has very good features of power density distribution control in the weld and HAZ. Power distribution of this heat source (Fig. 2) is formulated as follows:

$$q_1 = \begin{cases} q_1(x,y,z) = \frac{6\sqrt{3}f_1 Q_A}{abc_1\pi\sqrt{\pi}} \times \exp\left(-3\frac{x^2}{c_1^2}\right) \times \exp\left(-3\frac{y^2}{a^2}\right) \times \exp\left(-3\frac{z^2}{b^2}\right) & \text{for} \quad x < x_o, \\ q_2(x,y,z) = \frac{6\sqrt{3}f_2 Q_A}{abc_2\pi\sqrt{\pi}} \times \exp\left(-3\frac{x^2}{c_2^2}\right) \times \exp\left(-3\frac{y^2}{a^2}\right) \times \exp\left(-3\frac{z^2}{b^2}\right) & \text{for} \quad x \geqslant x_o \end{cases}, \tag{7}$$

where a, b, c_1 and c_2 are set of axes defining front ellipsoid and rear ellipsoid, f_1 and f_2 ($f_1 + f_2 = 2$) represent distribution of the source energy at the front and the rear section of the source, thus resultant distribution of the source energy is total sum described as $Q_1(x,y,z) = q_1(x,y,z) + q_2(x,y,z)$ and $Q_A = \eta_A IU$ is the arc heat source power, where I is a current intensity, U is a voltage and η_A is an efficiency of electric arc.

In the laser beam welding absorbed laser light vaporizes material and forms a "keyhole" that contains ionized vapor. Two mechanisms of Fresnel absorption and inverse Bremsstrahlung absorption are the cause of energy absorption by the material and the immediate transport of the heat below the surface of the workpiece [25,26]. Due to complexity of phenomena researchers are focused on plasma formation during laser beam welding [26–28] or laser beam heat source is considered in engineering practice as Gaussian-like simplified volumetric heat source [13,17,22]. In this study universal cylindrical-involution-normal (CIN) [22] heat source is used. This heat source model allows for modeling of variety concentrated volumetric heat source shapes with the relation between heat source power density and material penetration depth taken into account (Fig. 3)

$$Q_2(r,z) = \frac{kK_z\eta_L Q_L}{\pi(1 - e^{(K_z s)})}e^{-(kr^2 + K_z z)}(1 - u(z - s)), \tag{8}$$

where Q_L is the laser beam power, η_L is a laser efficiency, r_0 is a beam radius and $r = \sqrt{x^2 + y^2}$ is a current radius, $K_z = 3/s$ is a heat source power exponent, $k = 3/r_0^2$ is a beam focus coefficient and s is the heat source beam penetration depth, $u(z - s)$ is a Heaviside function.

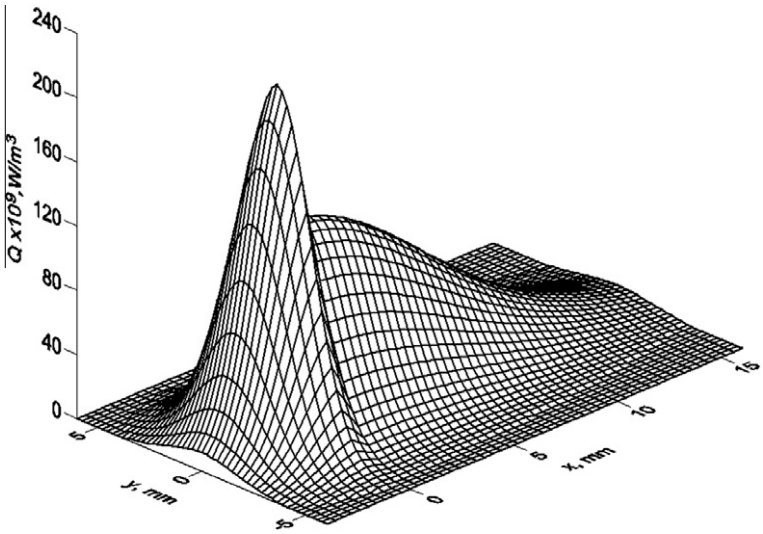

Fig. 2. Goldak's heat source distribution at the top surface ($z = 0$) of welded sheets. Heat source parameters are: $I = 288$ A, $U = 25$ V, $a = 4$ mm, $b = 2$ mm, $c_1 = 4$ mm, $c_2 = 16$ mm, $f_1 = 0.6$, $f_2 = 1.4$.

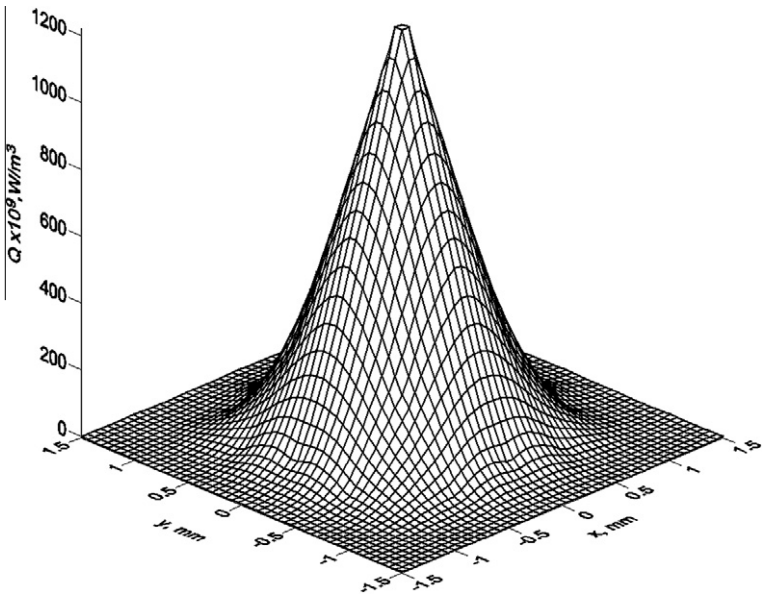

Fig. 3. CIN heat source power distribution at the top surface ($z = 0$) of welded sheets. Heat source parameters are: $Q_L = 3200$ W, $r_0 = 1$ mm, $s = 7$ mm.

In hybrid welding electric arc and laser beam are acting in a single process. The mutual influence of two heat sources improves melting efficiency by increasing the laser irradiation absorptivity caused by preheating and partial melting of workpiece surface by the arc as well as interaction of laser induced plasma with arc plasma [29,30]. In this work arc + laser hybrid heat source distribution (Fig. 4) is considered as a product of "double ellipsoidal" Goldak's model and CIN model ($Q_1 + Q_2$).

2.3. Solidification and evaporation models

Phase transformations due to material's state changes are taken into consideration in transient heat transfer equation. Effective heat capacity C_{ef} bellow solidus temperature is a product of density and specific heat in solid state. Between solidus and liquidus temperatures, the latent heat of fusion is included into the effective heat capacity [19,24], with assumed linear approximation of porosity coefficient, defined as:

$$C_{ef}(T) = \rho_{SL} c_{SL} + \rho_S \frac{H_L}{T_L - T_S} \quad \text{for} \quad T \in [T_S; T_L], \tag{9}$$

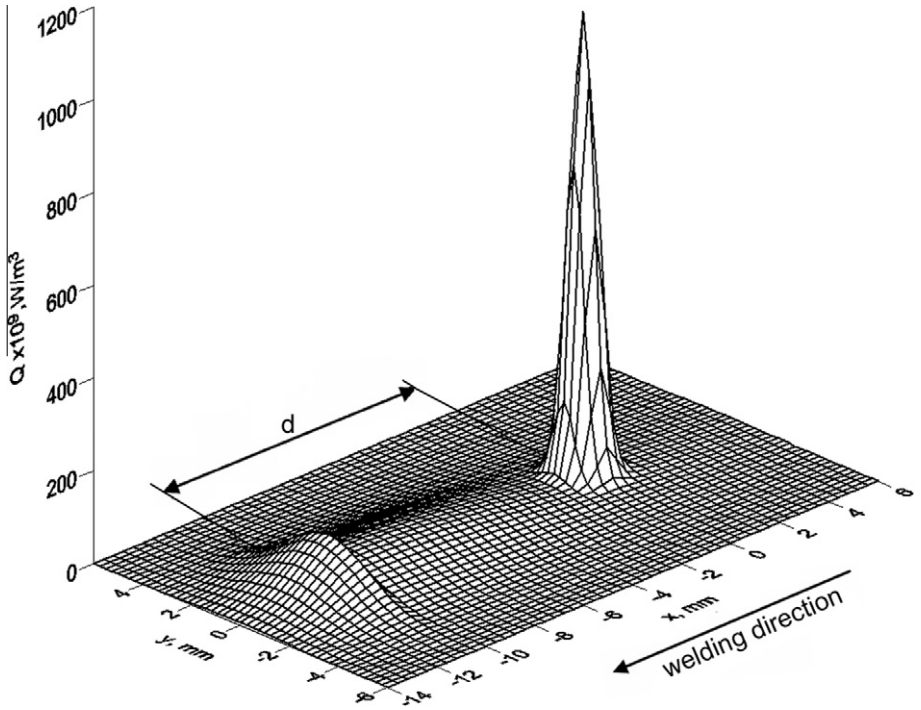

Fig. 4. Hybrid heat source power distribution at top surface ($z = 0$) of welded joint.

where T_s and T_L are solidus and liquidus temperatures respectively, H_L is a latent heat of fusion, $c_{SL}\rho_{SL} = c_S\rho_S(1 - f_l) + c_L\rho_L(f_l)$ is the product of density and specific heat in the mushy zone.

Between liquidus temperature and boiling point of steel the effective heat capacity is a product of density and specific heat in liquid state. Assuming full equilibrium of metal evaporation pressure in the "keyhole" and shielding gases pressure, and linear approximation of a liquid phase $f_{l-g} \in [0; 1]$ between the boiling point and maximum temperature, the effective heat capacity in temperatures exceeding boiling point is defined as follows:

$$C_{ef}(T) = \rho_L c_L + \frac{\rho_L H_b}{T_{\max} - T_b} \quad \text{for} \quad T \geqslant T_b, \tag{10}$$

where T_b is a boiling point of steel, T_{max} is a maximum temperature, H_b is a latent heat of evaporation.

3. Numerical solutions

Differential equations describing thermal phenomena in discussed welding processes are numerically solved using projection method with finite volume method (FVM) [17,19,31]. The spatial variables are discretized using staggered grid to avoid odd–even decoupling between the pressure and velocity. Elementary control volume is shown in Fig. 5. Velocity components are calculated at nodal points placed in the middle of each control volume face, while the pressure, density and temperature are calculated at the centre of control volume.

In the first step of the projection equation (4) is explicitly solved without momentum changes due to pressure forces. For elementary control volume differential form of momentum equation is described as follows:

$$\begin{aligned}
u^*_{i+1/2,j,k} &= u^s_{i+1/2,j,k} + \Delta t^s \left(-(A_x)^s_{i+1/2,j,k} + (f_x)^s_{i+1/2,j,k} \frac{2}{\rho^s_{i+1,j,k} + \rho^s_{i,j,k}} ((D_x)^s_{i+1/2,j,k} + (S_x)^s_{i+1/2,j,k}) \right), \\
v^*_{i,j+1/2,k} &= v^s_{i,j+1/2,k} + \Delta t^s \left(-(A_y)^s_{i,j+1/2,k} + (f_y)^s_{i,j+1/2,k} \frac{2}{\rho^s_{i,j+1,k} + \rho^s_{i,j,k}} ((D_y)^s_{i,j+1/2,k} + (S_y)^s_{i,j+1/2,k}) \right), \\
w^*_{i,j,k+1/2} &= w^s_{i,j,k+1/2} + \Delta t^s \left(-(A_z)^s_{i,j,k+1/2} + (f_z)^s_{i,j,k+1/2} \frac{2}{\rho^s_{i,j,k+1} + \rho^s_{i,j,k}} ((D_z)^s_{i,j,k+1/2} + (S_z)^s_{i,j,k+1/2}) \right),
\end{aligned} \tag{11}$$

where $\mathbf{v}^* = (u^*, v^*, w^*)$ is the velocity calculated from changes of velocity $\mathbf{v}^s$ resulting from advection $A_\alpha = (A_x, A_y, A_z)$, viscosity $D_\alpha = (D_x, D_y, D_z)$, source term $f_\alpha = (f_x, f_y, f_z)$ and flow through porosity medium $S_\alpha = (S_x, S_y, S_z)$.

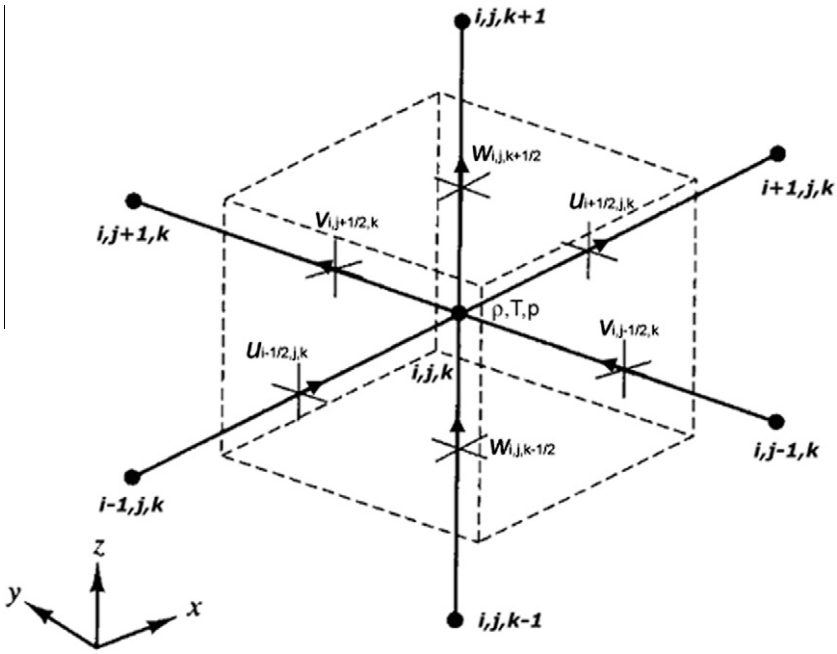

Fig. 5. Elementary control volume in staggered grid.

Central difference quotients derived for staggered grid were used to calculate each term in Eq. (11). In the second step the projection $\mathbf{v}^*$ onto velocity vector $\mathbf{v}^{s+1} = (u^{s+1}, v^{s+1}, w^{s+1})$ is made using the following equation:

$$
\begin{aligned}
u^{s+1}_{i+1/2,j,k} &= u^{*}_{i+1/2,j,k} - \left(\frac{2\Delta t^s}{\rho^s_{i+1,j,k} + \rho^s_{i,j,k}}\right)\frac{p_{i+1,j,k} - p_{i,j,k}}{h_x},\\
v^{s+1}_{i,j+1/2,k} &= v^{*}_{i,j+1/2,k} - \left(\frac{2\Delta t^s}{\rho^s_{i,j+1,k} + \rho^s_{i,j,k}}\right)\frac{p_{i,j+1,k} - p_{i,j,k}}{h_y},\\
w^{s+1}_{i,j,k+1/2} &= w^{*}_{i,j,k+1/2} - \left(\frac{2\Delta t^s}{\rho^s_{i,j,k+1} + \rho^s_{i,j,k}}\right)\frac{p_{i,j,k+1} - p_{i,j,k}}{h_z},
\end{aligned}
\tag{12}
$$

with the assumption of fulfilling the continuity equation in the differential form

$$
\frac{u^{s+1}_{i+1/2,j,k} - u^{s+1}_{i-1/2,j,k}}{h_x} + \frac{v^{s+1}_{i,j+1/2,k} - v^{s+1}_{i,j-1/2,k}}{h_y} + \frac{w^{s+1}_{i,j,k+1/2} - w^{s+1}_{i,j,k-1/2}}{h_z} = 0, \tag{13}
$$

where h_x, h_y, h_z are the dimensions of control volume, Δt^s is a time step from the time s.

Eqs. (12) and (13) are deposited in a single Poison equation used to find the pressure, at which the velocity at the new time step is divergence free.

After velocity field of melted material is obtained, temperature field in welded workpiece is calculated on the basis of the solution of heat transfer equation expressed in the differential form as follows:

$$
\begin{aligned}
T^{s+1}_{i,j,k} = T^s_{i,j,k} &+ \frac{\tilde{Q}\Delta t^s}{C_{ef}} - \left(u\frac{T^s_{i+1} - T^s_{i-1}}{2h_x} + v\frac{T^s_{j+1} - T^s_{j-1}}{2h_y} + w\frac{T^s_{k+1} - T^s_{k-1}}{2h_z}\right)\Delta t^s\\
&+ \frac{\Delta t^s}{C_{ef}}\left(\frac{\lambda^s_{i+1} - \lambda^s_{i-1}}{2h_x}\frac{T^s_{i+1} - T^s_{i-1}}{2h_x} + \lambda^s_i\frac{T^s_{i-1} - 2T^s_i + T^s_{i+1}}{(h_x)^2}\right) + \frac{\Delta t^s}{C_{ef}}\left(\frac{\lambda^s_{j+1} - \lambda^s_{j-1}}{2h_y}\frac{T^s_{j+1} - T^s_{j-1}}{2h_y} + \lambda^s_j\frac{T^s_{j-1} - 2T^s_j + T^s_{j+1}}{(h_y)^2}\right)\\
&+ \frac{\Delta t^s}{C_{ef}}\left(\frac{\lambda^s_{k+1} - \lambda^s_{k-1}}{2h_z}\frac{T^s_{k+1} - T^s_{k-1}}{2h_z} + \lambda^s_k\frac{T^s_{k-1} - 2T^s_k + T^s_{k+1}}{(h_z)^2}\right).
\end{aligned}
\tag{14}
$$

Because forward Euler integration scheme is used in calculations as well as central difference quotients, quality of the results depends on the conditions of stability. Time step constraints and additional stabilization methods for high Peclet numbers [31] are taken into account in solution algorithms to ensure proper quality of the results.

4. Results and discussion

Computer simulation of laser beam welding and laser-arc hybrid welding processes was performed for sheets made of S355 steel. The dimensions of the sheets are $150 \times 30 \times 4$ mm. Analyzed domain was discretized by staggered grid with the spatial step set to 0.1 mm. Thermo-physical parameters used in calculations are summarized in Table 1 [32].

Laser beam welding simulation was performed with following technological parameters: welding speed $v = 1.2$ m/min, laser beam power $Q_L = 3800$ W, laser beam radius $r_0 = 1$ mm, penetration deep $s = 5$ mm and laser efficiency $\eta_L = 85\%$ in agreement with the data given in [33]. The simulation of laser-arc hybrid welding process in geometrical set-up with leading electric arc in the tandem was performed assuming the same laser beam parameters as in the simulation of single laser beam

Table 1
Thermo-physical parameters assumed in computer simulations.

Nomenclature	Symbol	Value
Solidus temperature	T_S	1750 K
Liquidus temperature	T_L	1800 K
Boiling point	T_b	3010 K
Ambient temperature	T_0	293 K
Specific heat of solid phase	c_S	650 J kg^{-1} K^{-1}
Specific heat of liquid phase	c_L	840 J kg^{-1} K^{-1}
Density of solid phase	ρ_S	7800 kg m^{-3}
Density of liquid phase	ρ_L	6800 kg m^{-3}
Latent heat of fusion	H_L	270×10^3 J kg^{-1}
Latent heat of evaporation	H_b	76×10^5 J kg^{-1}
Thermal conductivity of solid phase	λ_S	45 W m^{-1} K^{-1}
Thermal conductivity of liquid phase	λ_L	35 W m^{-1} K^{-1}
Convective heat transfer coefficient	α	50 W m^{-2} K^{-1}
Boltzmann's constant	σ	5.67×10^{-8} W m^{-2} K^{-4}
Thermal expansion coefficient	β_T	4.95×10^{-5} K^{-1}
Surface radiation emissivity	ε	0.5
Dynamic viscosity	μ	0.006 kg m^{-1} s^{-1}
Solid particle average diameter	d_0	0.0001 m

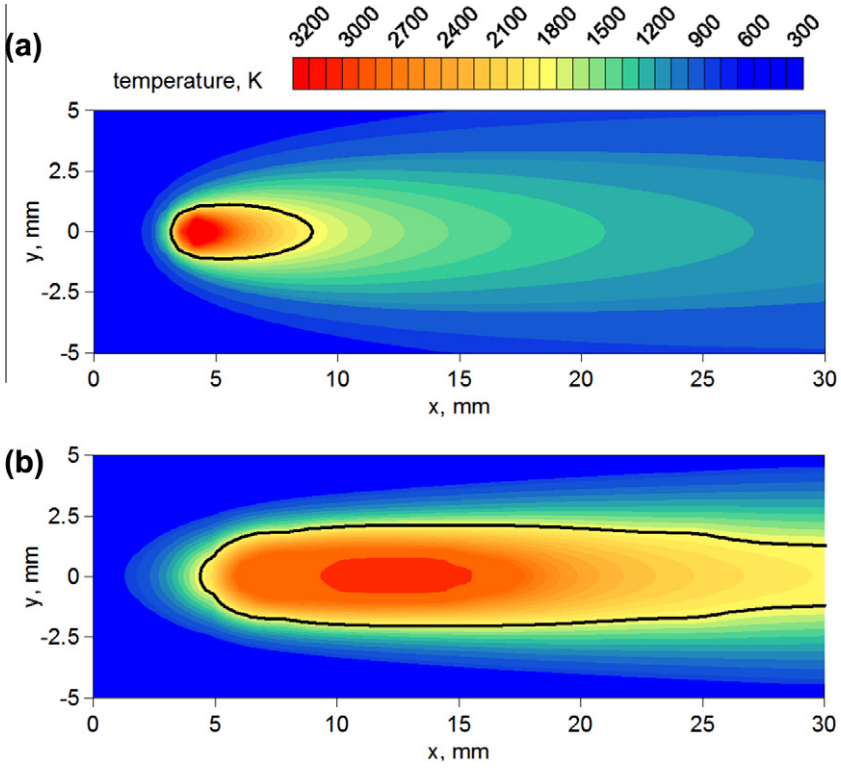

Fig. 6. Temperature distribution at the top surface ($z = 0$) of the joint welded by (a) laser beam and (b) laser-arc hybrid method.

welding. Electric arc heat source parameters were set to: arc current $I = 310$ A, welding voltage $U = 31.8$ V. Distance between arc torch and laser beam focal point was set to $d = 5$ mm and welding speed $v = 2.6$ m/min. According to research on thermal efficiency of hybrid welding process, performed in [34,35] it was assumed that hybrid heat source efficiency consist of arc efficiency $\eta_A = 75\%$ and laser efficiency $\eta_L = 85\%$.

Figs. 6 and 7 present temperature distribution in laser beam and laser-arc hybrid butt welding respectively, at the top surface (Fig. 6) of the joint (from the face of the weld, $z = 0$) and in longitudinal section (Fig. 7), in the middle of heat sources activity zone ($y = 0$). Solid line points out the welding pool boundary (solidus isotherm).

It is observed that additional heat source in hybrid welding changes material melting mechanism and geometry of the welding pool (Fig. 6). As shown in longitudinal section of hybrid welded joint (Fig. 7(b)), when electric arc is the leading heat source in the tandem, this heat source melts upper parts of the workpiece, which allows for a better material penetration by the laser beam.

Melted material velocity field in longitudinal section of laser and hybrid welded butt-joint is presented in Fig. 8. As shown in this figure velocity field in the welding pool reaches maximum values in the laser beam activity zone.

Temperature field (at the right side) and melted material velocity field (at the left side) in the cross section of laser and hybrid welded joint is illustrated in Fig. 9. Solid line points out the melted zone boundary, whereas dashed line marks the boundary of HAZ ($T_g \approx 1000$ K).

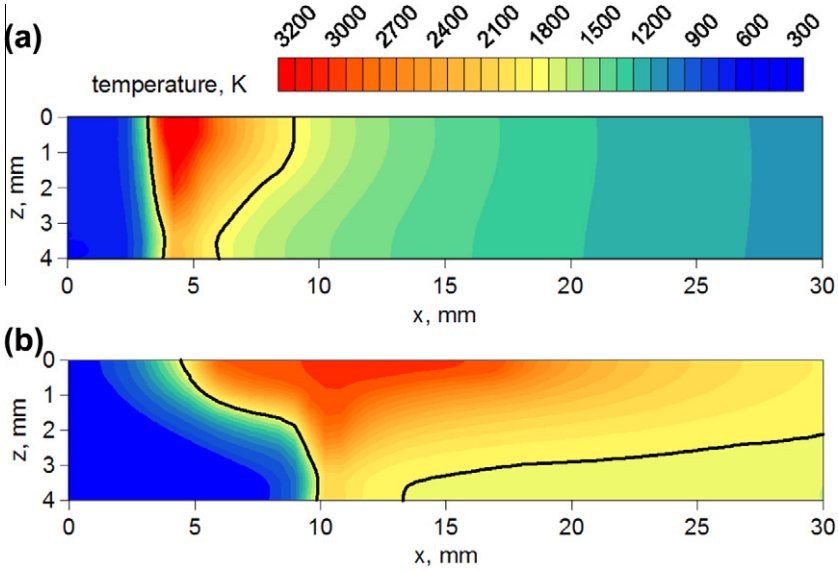

Fig. 7. Temperature distribution in the longitudinal section ($y = 0$) of the joint welded by (a) laser beam and (b) laser-arc hybrid method.

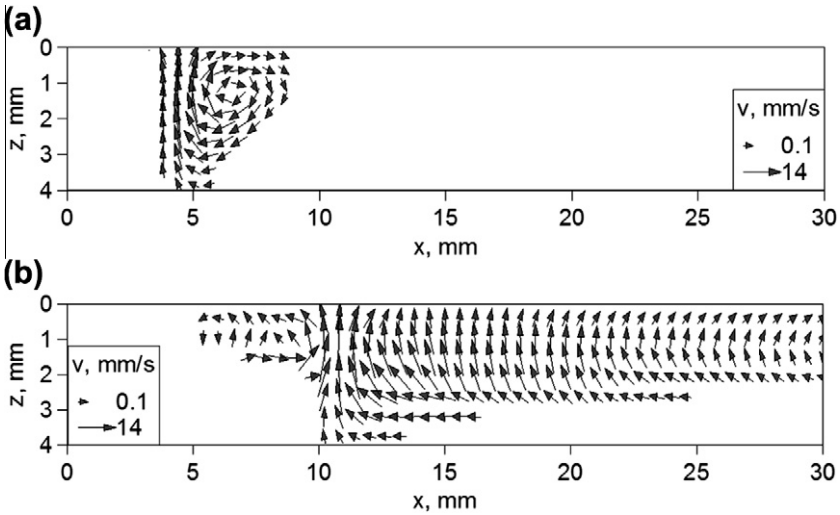

Fig. 8. Liquid material velocity field in the longitudinal section ($y = 0$) of the joint welded by (a) laser beam and (b) laser-arc hybrid method.

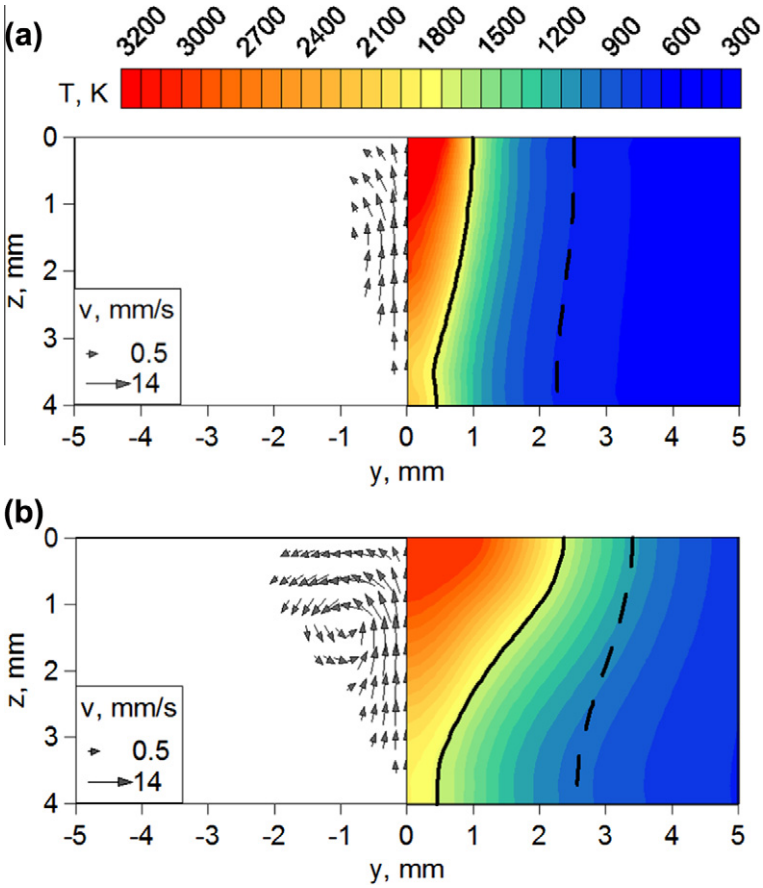

Fig. 9. Temperature field (at the right side) and liquid material velocity field (at the left side) in the cross section of the joint welded by (a) laser beam and (b) laser-arc hybrid method.

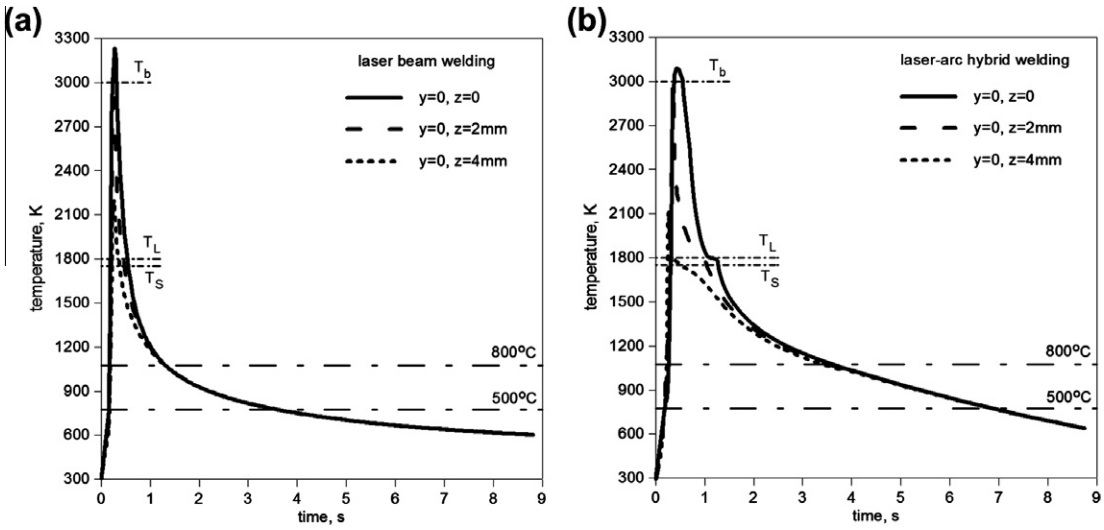

Fig. 10. Thermal cycles for chosen points in the middle ($y = 0$) of heat sources plane in joint welded by (a) laser beam and (b) laser-arc hybrid method.

Calculated temperature field in the cross section of the joint (Fig. 9) allows for determination of weld and heat affected zone geometry. It is observed that motion of melted material in the welding pool has a significant influence on the weld shape, especially in the hybrid welding process. Maximum velocity of melted steel is reached in the middle of heat sources

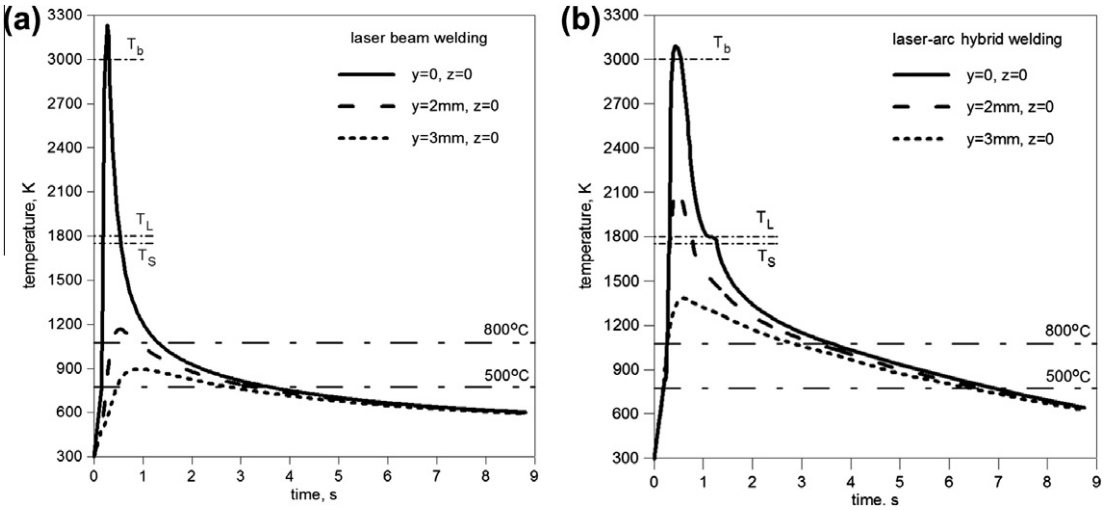

Fig. 11. Thermal cycles for chosen points at the top surface ($z = 0$) of the joint welded by (a) laser beam and (b) laser-arc hybrid method.

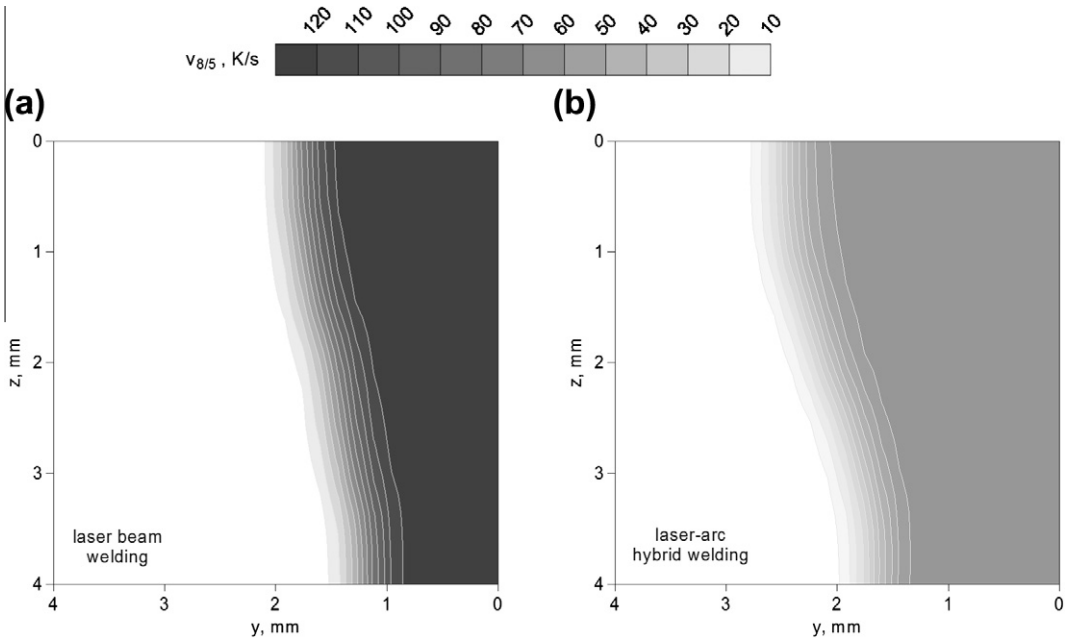

Fig. 12. Cooling rates in cross section of the joint welded by (a) single laser beam and (b) laser-arc hybrid method.

activity zone. To achieve full material penetration in laser beam welding, welding speed was decreased to 1.2 m/min. In hybrid welding process the distance between the arc and laser beam $d = 5$ mm is sufficient for synergy effect due to interaction of both heat sources in the welding pool.

Figs. 10 and 11 present thermal cycles for chosen points in laser beam welding and hybrid welding respectively. Solidus, liquidus and boiling temperatures are marked as well as the temperature range [800 ÷ 500] °C where cooling rates ($v_{8/5}$) are estimated – the base factor determining the kinetics of phase transformations in solid state and allowing the prediction of microstructure composition in the weld and HAZ. It can be noticed that heat generated during melting and solidification of steel affects temperature distribution between T_S and T_L temperatures (mushy zone). Cooling rates estimated in temperature range [800 ÷ 500] °C are presented in Fig. 12 in the cross section of welded joints.

After solidification, laser welded joint is rapidly cooled to the ambient temperature which results in partial hardening of the weld and HAZ. The comparison of cooling rates distribution (Fig. 12) shows that hybrid welding process extends the cooling time which contributes to the reduction of hardening structures and improvement in weld quality.

Hybrid welding experiment was performed at Institute of Welding in Gliwice to verify the correctness developed models. In the experiment CO_2 laser was used with maximum power up to 3.8 kW and semi-automatic welder with MIG/MAG weld-

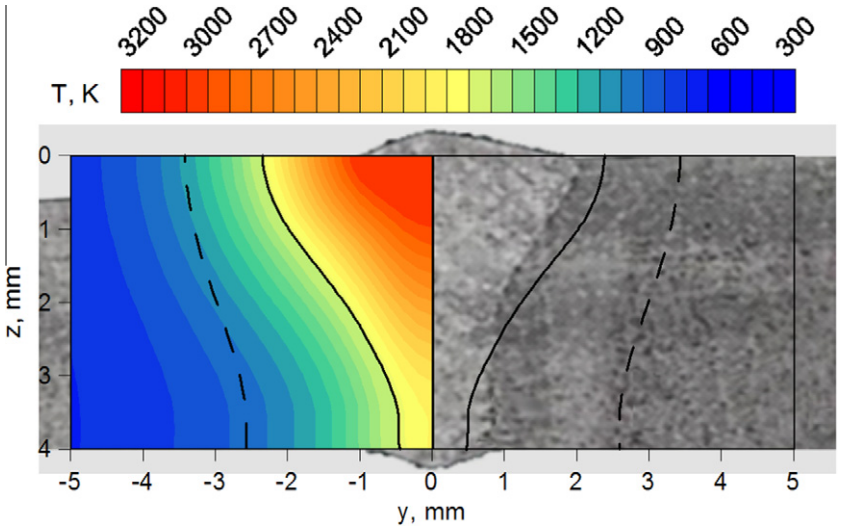

Fig. 13. Cross section of hybrid welded joint with marked calculated melted zone and HAZ.

ing torch. Hybrid butt welding of S355 steel sheets with dimensions 150 × 30 × 4 mm was made with leading electric arc in the process. Technological parameters were set to: welding speed v = 2.6 m/min, laser beam power Q_L = 3800 W, arc current I = 310 A, arc voltage U = 31.8 V, feed rate 10 m/min, laser-to-arc distance $d \approx 5$ mm, shielding gases – helium 8 l/min used for laser and argon/helium (50%/50%) 12 l/min used for arc. Fig. 13 shows the comparison between results of hybrid welding simulation (from left) and experimental results (from right) in the cross section of the weld with marked fusion zone and HAZ boundary.

5. Conclusions

This paper presents mathematical model and numerical solutions of thermal phenomena in laser beam and laser-arc hybrid welding processes. Three-dimensional numerical model of temperature field in welded joint takes into account the motion of liquid metal in the welding pool and latent heat associated with the material's state change. The results of numerical analysis include: temperature field and velocity field of melted steel in the welding pool. On the basis of calculated temperature distribution the evaluation of the size and shape of the weld and heat affected zone is possible as well as the estimation of cooling rates, depending on heat source type and process parameters.

Basing on preformed numerical analysis the following conclusions are derived:

- The use of laser-arc hybrid heat source allows doubling the welding speed (v = 2.6 m/min) compared with a single laser beam welding (v = 1.2 m/min) for the same welded joint and identical laser beam parameters used in both welding techniques. The efficiency of hybrid welding can be interesting especially for welding of long workpieces.
- Diversified nature of liquid material motion in the fusion zone created by hybrid heat source and a single laser beam (Figs. 8 and 9) implies a different material melting mechanism. Greater melting efficiency in hybrid welding can have a big impact on the quality of the weld. However, confirmation of this conclusion requires metallographic examination.
- Hybrid welding reduces cooling rates in the range of phase transformations in solid state in comparison to cooling rates achieved during laser welding (Figs. 10–12) which provides reduction of joint hardening in the heat affected zone. This feature of hybrid welding is very important because one of major problems of laser welding is the hardening of steel in the weld and HAZ.

Presented mathematical models and numerical solutions allow determining a proper set of process parameters such as welding speed, heat sources relative arrangement and selection of heat sources power ensuring desired geometry of the weld and HAZ with a good quality of the joint. The accuracy of numerically obtained results with the experimental results indicates the correctness of elaborated models.

References

[1] C. Dawes, Laser Welding, Abington Publishing, New York, 1992.
[2] K. Abderrazak, S. Bannour, H. Mhiri, G. Lepalec, M. Autric, Numerical and experimental study of molten pool formation during continuous laser welding of AZ91 magnesium alloy, Comp. Mat. Sci. 44 (2009) 858–866.
[3] J. Pilarczyk, M. Banasik, J. Dworak, S. Stano, Technological applications of laser beam welding and cutting at the Instytut Spawalnictwa, Przeglad Spawalnictwa 5–6 (2006) 6–10.

[4] P. Seyffarth, I.V. Krivtsun, Laser-Arc Processes and their Applications in Welding and Material Treatment, Taylor & Francis, USA, 2002.
[5] C. Bagger, F.O. Olsen, Review of laser hybrid welding, J. Laser Appl. 17 (2005) 2–14.
[6] J. Pilarczyk, M. Banasik, J. Dworak, S. Stano, Hybrid welding using laser beam and electric arc, Przeglad Spawalnictwa 10 (2007) 44–48.
[7] U. Dilthey, A. Wieschemann, Prospects by combining and coupling laser beam and arc welding processes, Weld. World 44 (2000) 37–46.
[8] Y.B. Chen, Z.L. Lei, L.Q. Li, L. Wu, Experimental study on welding characteristics of CO_2 laser TIG hybrid welding process, Sci. Technol. Weld. Joining 11 (2006) 403–411.
[9] M. Adak, N.R. Mandal, Numerical and experimental study of mitigation of welding distortion, Appl. Math. Model. 34 (2010) 146–158.
[10] Hee Seon Bang, Han Sur Bang, You Chul Kim, Sung Min Joo, Analysis of residual stress on AH32 butt joint by hybrid CO2 laser-GMA welding, Comp. Mat. Sci. 49 (2010) 217–221.
[11] R. Rai, S.M. Kelly, R.P. Martukanitz, T.A. Debroy, Convective heat-transfer model for partial and full penetration keyhole mode laser welding of a structural steel, Metall. Mater. Trans. A 39A (2008) 98–112.
[12] A. Bokota, W. Piekarska, Modeling of residual stresses in laser welding, Paton Weld. J. 6 (2008) 19–24.
[13] L. Han, F.W. Liou, Numerical investigation of the influence of laser beam mode on melt pool, Int. J. Heat Mass Trans. 47 (2004) 4385–4402.
[14] V.I. Makhnenko, G.Y. Saprykina, Role of mathematical modelling in solving problems of welding dissimilar steels, Paton Weld. J. 3 (2002) 14–25.
[15] A. Anca, A. Cardona, J. Risso, V.D. Fachinotti, Finite element modeling of welding processes, Appl. Math. Model. 35 (2011) 688–707.
[16] A. De, T. DebRoy, Reliable calculations of heat and fluid flow during conduction mode laser welding through optimization of uncertain parameters, Weld. J. 84 (2005) 101–111.
[17] G.A. Taylor, M. Hughes, N. Strusevich, K. Pericleous, Finite volume methods applied to the computational modelling of welding phenomena, Appl. Math. Model. 26 (2002) 309–320.
[18] Z.H. Rao, J. Hu, S.M. Liao, H.L. Tsai, Modeling of the transport phenomena in GMAW using argon–helium mixtures. Part II – The metal, Int. J. Heat Mass Trans. 53 (2010) 5722–5732.
[19] W. Piekarska, M. Kubiak, Three-dimensional model for numerical analysis of thermal phenomena in laser-arc hybrid welding process, Int. J. Heat Mass Trans. 54 (2011) 4966–4974.
[20] J. Zhou, H.L. Tsai, Modeling of transport phenomena in hybrid laser – MIG keyhole welding, Int. J. Heat Mass Trans. 51 (2008) 4353–4366.
[21] J.A. Goldak, Computational Welding Mechanics, Springer, New York, 2005.
[22] E. Ranatowski, Thermal modelling of laser welding. Part I: The physical basis of laser welding, Adv. Mater. Sci. 1 (2003) 34–40.
[23] B. Nedjar, An enthalpy-based finite element method for nonlinear heat problems involving phase change, Comput. Struct. 80 (2002) 9–21.
[24] S. Jana, S. Ray, F. Durst, A numerical method to compute solidification and melting processes, Appl. Math. Model. 31 (2007) 93–119.
[25] X. Jin, L. Li, Y. Zhang, A study of fresnel absorption and reflections in the keyhole in deep penetration laser welding, J. Phys. D: Appl. Phys. 35 (2002) 2304–2310.
[26] D.V. Bedenko, O.B. Kovalev, I.V. Krivtsun, Simulation of plasma dynamics in a keyhole during laser welding of metal with deep penetration, J. Phys. D: Appl. Phys. 43 (10) (2010) 105501.
[27] M. Beck, P. Berger, H. Hugel, The effect of plasma formation on beam focusing in deep penetration welding with CO_2 lasers, J. Phys. D: Appl. Phys. 28 (1995) 2430–2442.
[28] V. Semak, A. Matsunawa, The role of recoil pressure in energy balance during laser materials processing, J. Phys. D: Appl. Phys. 30 (1997) 2541–2552.
[29] L. Liu, M. Chen, Interaction between laser and arc plasma during laser-arc hybrid welding of magnesium alloy, Optic. Laser. Eng. 49 (2011) 1224–1231.
[30] Y.T. Cho, W.I. Cho, S.J. Na, Numerical analysis of hybrid plasma generated by Nd:YAG laser and gas tungsten arc, Optic. Laser. Tech. 43 (2011) 711–720.
[31] S.V. Patankar, Numerical Heat Transfer and Fluid Flow, Taylor & Francis, USA, 1990.
[32] W. Piekarska, Numerical analysis of thermomechanical phenomena during laser welding process. The temperature field, phase transformations and stresses, Monograph series 135, Częstochowa, 2007.
[33] P.W. Fuerschbach, Measurements and prediction of energy transfer efficiency in laser beam welding, Weld. J. 75 (1996) 24–34.
[34] B. Hu, G. den Ouden, Synergetic effects of hybrid laser/arc welding, Sci. Technol. Weld. Joining 10 (2005) 427–431.
[35] E.W. Reutzel, S.M. Kelly, R.P. Martukantiz, M.M. Bugarewicz, P. Michaleris, Laser-GMA hybrid welding: Process monitoring and thermal modeling, in: Proc. of the 7th International Conference Trends in Welding Research, Pine Mountain, USA, 2005.